

## Deformation monitoring of noise barriers with profile laser scanning

Florian Schill, Anna Sviridova, Andreas Eichhorn

TU Darmstadt, Institute of Geodesy - Geodetic Measuring Systems and Sensor Technology, Franziska-Braun-Straße 7, 64287 Darmstadt, Germany, ([schill@geod.tu-darmstadt.de](mailto:schill@geod.tu-darmstadt.de))

**Key words:** deformation monitoring; noise barrier; railway; profile scanner; spatial clustering; B-splines; accelerometer; inductive displacement sensor

### ABSTRACT

Noise barriers along railway tracks are exposed to great load changes, as a result of the strongly varying pressure field induced by passing trains. Especially at high speed tracks the dynamic load effects can lead to huge stress on the structure, because high and low pressure sections follow directly on to each other. The deformation monitoring of noise barriers is usually realised with conventional sensors for the monitoring of supporting structures (accelerometers or inductive displacement sensors), which require a lot of installation effort and yields only information at discrete measurement points. With the usage of a profile scanner the installation effort can be reduced, and furthermore, it is possible to generate added value in information about the structure, due to its high profile wise spatial resolution. Compared to conventional sensors the profile scanner can generate qualitatively comparable results with less effort and therefore opens up new possibilities for the efficient monitoring of noise barriers.

### I. INTRODUCTION

Noise is the biggest environmental problem for the otherwise environmentally friendly rail transport sector. Noise emissions are therefore becoming one of the limiting factors in the operation of the rail network (Thompson, 2008). In order to counteract this problem, the expansion of noise protection measures such as noise barriers is becoming increasingly important (Schulte-Werning et al., 2006).

During their lifetime, noise barriers are regularly exposed to instationary dynamic loads from the aerodynamic pressure and suction of passing trains. This can add up to millions of load cycles. Especially on high-speed tracks, the associated loads place very high demands on the used noise protection elements (Hoffmeister, 2007).

Accordingly, the functionality of noise barriers is an important factor for safe rail operations, as damaged elements can pose a threat or hindrance to rail traffic. In order to detect this at an early stage and be able to take appropriate countermeasures, an efficient deformation monitoring concept for noise protection measures with regard to their dynamic deformation behaviour in regular railway operation is required.

Present measurement concepts favour conventional sensors (accelerometers, inductive displacement sensors or strain gauges) to monitor noise barriers (Tokunaga et al., 2014).

The use of accelerometers is thereby mostly motivated by the fact that they can be mounted on the structure almost without any preconditions, i. e. no measuring base is required. However, in order to derive deformations, the acceleration time series must be integrated twice, which again pose numerical problems.

In addition, the derivation of uncertainties for twice integrated acceleration measurements is not trivial.

For the use of inductive displacement sensors, a stable measuring base is needed, decoupled from the acting forces, which is a very complex task at noise barrier heights of 4 m and more.

In addition, both measurement systems have the disadvantage that they need to be attached to the noise barrier and the generated measurement information is therefore limited to discrete points.

With the use of a profile scanner we present a novel measurement concept for the efficient acquisition of noise barrier deformations in regular railway operation. This article shows that using the contactless measurement method of a profile scanner, the measurement effort is greatly reduced and an added value can be generated due to the high spatial resolution.

In the following section, the proposed measurement system is introduced and its key parameters are presented. Section 3 shows the comparison of the measurement concepts of a profile scanner, inductive displacement sensors and accelerometers as part of a preliminary investigation for the deformation monitoring of noise barriers. In Section 4 an initial investigation of a noise barrier using profile scanning is presented and the generated added value is addressed.

### II. MEASUREMENT SYSTEM

The measurement system presented in this article is based on the Z+F Profiler 9012, see Figure 1, which is a profile scanner operating according to the phase measurement principle. The main area of operation is basically mobile platforms. The application of the profile scanner for the monitoring of noise barriers is a

reversal of its original task, since in this case a moving object is sampled from a static platform, e. g. (Schill and Eichhorn, 2016; Schill and Eichhorn, 2017; Wujanz et al., 2018). The laser beam is passed in one direction over the measuring object, with a repetition rate of 50 Hz, 100 Hz or 200 Hz. The manufacturer specifies a distance measurement range between 0.3 m and 119 m with a maximum data recording rate of 1 million points per second (Zoller+Fröhlich, 2019).

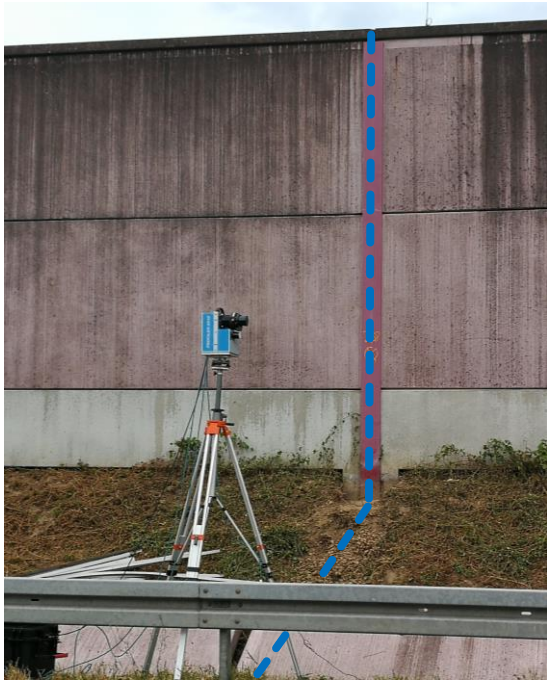


Figure 1. Profile scanner during the monitoring of a noise barrier.

As a result, a two-dimensional point cloud is created, which is arranged in measurement profiles. Every individual measurement profile contains up to 20.000 measuring points per 360 degree, see Figure 2. In addition, each measurement point receives a precise time information with an uncertainty ( $3\sigma$ ) of 60 ns due to the integration of a u-blox Precision Timing GPS-Module (Schill, 2018; u-blox, 2019).

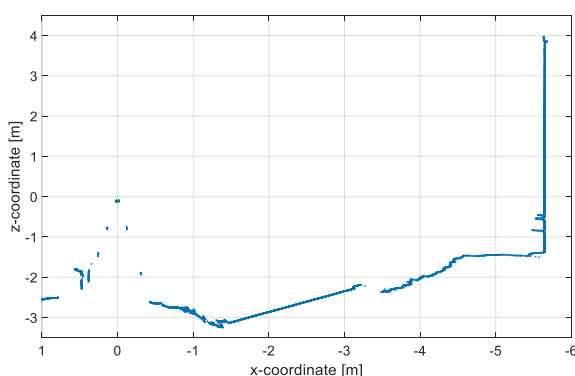


Figure 2. Exemplary measurement profile during the monitoring of a noise barrier.

Due to the modified scope of application of the profile scanner, constructive adaptations had to be

developed. This is, among other things, a tripod adapter that allows the profile scanner to be mounted in a stable manner in different orientations in relation to the measuring object, see Figure 1. A detailed overview of the developed adaptations and further studies of the individual profile scanner components can be found in (Schill, 2018).

Furthermore, there is no standard data processing software for the use of the profile scanner to monitor supporting structures. A special processing concept has therefore been developed that can take advantage of the high spatial and temporal measurement resolution of the profile scanner (Schill, 2018).

### III. PRELIMINARY INVESTIGATION

#### A. Configuration

The preliminary investigations were carried out using a model of a footbridge, see the schematic section in Figure 3. The bridge model is located on the campus of TU Darmstadt and was designed by the Institute of Structural Mechanics and Design (ISMD). In principle, the model is intended, among other things, for studies on human-structure-interaction (Firus et al., 2018).

The structure of the bridge consists of two steel beams with a span of 13.2 m. 13 prefabricated concrete panels are placed on the steel beams. In order to prevent the panels from slipping, there is a thin elastomer layer (5 mm) between the panels and the steel beams. The bridge has a total weight of 12 tonnes, a fundamental frequency of about 2 Hz and a modal damping of 0.3 %.

The vibration stimulation was triggered by people walking across the bridge with a step frequency of 2Hz, matching the fundamental frequency of the bridge.

Due to the dimensions, material and deformation behaviour the footbridge model is well suited for the preliminary investigation related to the monitoring of noise barriers. Furthermore the horizontal orientation enables the usage of inductive displacement sensors without the need for a separate measuring base.

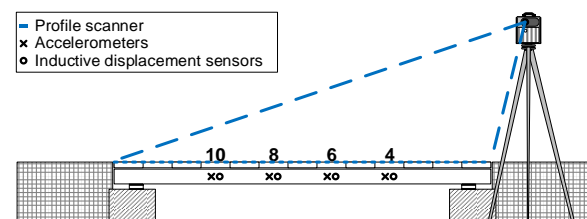


Figure 3. Placement and numbering of the used sensors.

As part of the comparison measurements, four inductive displacement sensors (HBM 1-WA/50MM-L) with a linearity deviation of  $\leq 0.2\%$  (equivalent to  $\leq 0.1$  mm for this configuration) and four piezoelectric accelerometers (PCB-TLD393B04) with a non-linearity of  $\leq 1\%$  were attached to the underside of the footbridge. The positioning is shown in Figure 3 along with the position of the profile scanner.

### B. Pre-processing of acceleration and profile scanner measurements

The comparison of the sensor time series is carried out on the basis of displacements since they are the main scope for the monitoring of noise barriers in this article. In this context the inductive displacement sensors are used as a reference for the preliminary investigation, due to their single point measurement precision.

For this comparison the measurement data of the accelerometers and the profile scanner have to be pre-processed as follows:

The measurements of the accelerometers have to be integrated twice in order to derive displacements. The fundamental problem that occurs during this integration is the inherent exponential gain of low frequency components (signal and noise) due to its characteristic frequency response, e. g. (Neitzel et al., 2007). To illustrate the problem of integration the results of a twice-integrated time series are shown in the upper diagrams of Figure 4. In this example an accelerometer measurement time series at bridge position 4 with a fundamental frequency of about 2 Hz and an expected maximum amplitude of approximately 5 mm is presented. The integration was performed with the trapezoidal rule.

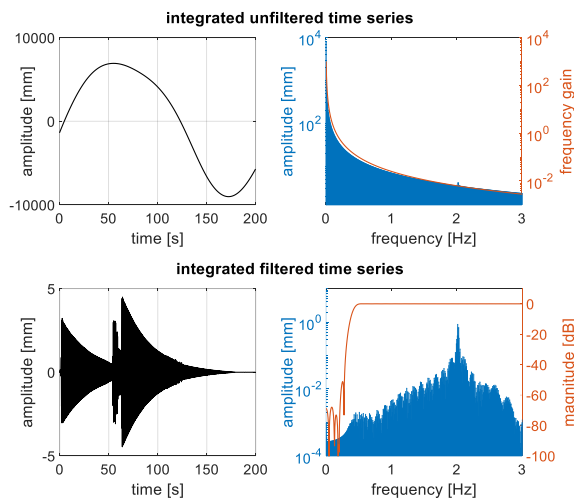


Figure 4. Exponential gain and filtering of the integrated accelerometer measurements.

The upper left diagram shows the twice integrated signal in the time domain, whereas the right diagram shows the low frequency part of the signal in the frequency domain up to 3 Hz. Both the theoretical frequency response of the double integration (red) and the discrete spectra of the integrated time series (blue) show the exponential gain in the frequency domain, which leads to the low frequency distortion of the resulting displacement signal.

To overcome this issue a high pass filtering has to be applied. Accordingly the lower diagrams of Figure 4 show the filtered signal on the left side in the time domain and on the right side the low frequency part of

the filtered signal (blue) in the frequency domain up to 3 Hz. In addition the frequency response of the used finite impulse response (FIR) high pass filter with a cutoff frequency of 0.4 Hz (red) is depicted. Numerical integration methods add the problem of unknown initial values see for example (Hwang et al., 2012), which causes additional low frequency components. In terms of avoiding this outcome, integration of the Fourier transform or usage of the trapezoidal rule with subtraction of the mean value after every integration step could be used.

Although the profile scanner measures the displacements directly, a pre-processing step is necessary. Since the profile scanner captures the entire bridge surface with at least 50 Hz, the bridge movement can be almost completely captured in space and time. However, only small spatial sections of the measurement profiles are relevant for the comparison with the results of the conventional sensors.

For this purpose, the measured profile points within those spatial units (angle ranges) are processed together with the aim of deriving a representative (e.g. mean value) for this part of the profile (spatial cluster). The explicit definition of the spatial cluster allows to determine directly which points of the measurement profile are included in the calculation of the representative. For comparison with the conventional sensors, the areas were selected symmetrically around the corresponding sensor positions.

### C. Comparison of the sensor time series

In the following the measurement time series at bridge position 4 are presented (see Figure 3), because the corresponding geometric measurement configuration is roughly the same that occurs when monitoring noise barriers. The displayed results of the preliminary investigation can therefore be considered representative for the monitoring of noise barriers.

Both diagrams in Figure 5 show the time series of the used sensors over a period of 180 seconds for bridge position 4.

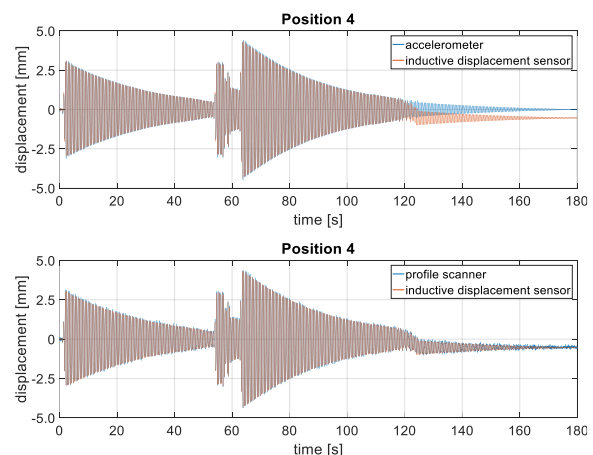


Figure 5. Time series of the sensor measurements for bridge position 4.

Since the inductive displacement sensor measurements are considered as the reference measurements, they are combined with the integrated accelerometer measurements in the upper diagram and with the profile scanner measurements in the lower diagram. Figure 6 complements this representation with the corresponding differences.

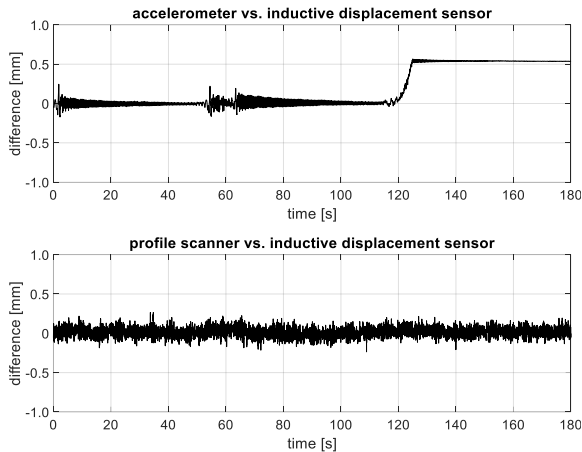


Figure 6. Differences of the time series from Figure 5.

The time series of differences between the integrated accelerometer and the inductive displacement sensor in the upper diagram in Figure 6 shows two different kinds of effects:

The more noticeable of the two effects occurs at approximately second 120, with an amplitude of 0.5 mm, a duration of 6 seconds and can therefore be characterized as a low frequency drift.

The upper diagram of Figure 5 shows the reason: The central oscillation position of the time series of the inductive displacement sensor is changing from 0 mm to -0.5 mm. This drift does not exist in the time series of the integrated accelerometer measurements, due to the filtering with the previously discussed FIR high pass filter in combination with the pre-processing of the accelerometer measurements.

The second visible effect in the differences matches with the displacement signal from Figure 5, meaning that larger amplitudes produce larger deviations. It can be observed that the absolute displacements in the integrated accelerometer time series are always slightly larger than the inductive displacement sensor registers. The proportionality of the difference amplitudes to the measured displacements indicate a scale factor between the time series. This scale factor is likely caused by non-linearities in the calibrated transfer function of the accelerometers or by undetected temperature influences. The effect is not limited to the time series at position 4, but occurs at all bridge positions and varies between +1% and +3%, depending on the sensor combination.

The preliminary results of this comparison illustrate, that the usage of accelerometers to derive displacement is prone to erroneous processing and in

principle problematic, due to the discussed issues in the low frequency area.

The comparison of the profile scanner with the inductive displacement sensor in the lower diagrams in Figure 5 and Figure 6 shows no significant systematic effects. If the difference time series depicted in the lower diagram of Figure 6 is assumed to be randomly distributed, a standard deviation for one difference results of  $\leq 0.1$  mm. This uncertainty is approximately the same, as the one derived for a representative of a spatial class and thus characterizes the displacements derived from the profile scanner measurements.

The entire comparison shows that profile scanner measurements can produce comparable results in recording displacements for the monitoring of noise barriers. Compared to the presented inductive displacement sensor, the installation effort is reduced considerably, due to the contactless measuring principle. This advantage is becoming even more important for the monitoring of noise barriers under real-world conditions, as the generation of a stable measurement basis, decoupled from the acting forces, is a major challenge with correspondingly increasing expense for installation.

In addition, the high spatial resolution of the profile scanner measurements generates an added value for the monitoring of noise barriers. Based on the profile wise capturing of the deformations along the structure, these outputs can be matched with load assumptions or spatially distributed measurements of the effective load. Thus, it is possible to verify the assumptions made about the spatially distributed transmission behaviour of the noise barrier.

#### IV. MONITORING OF A NOISE BARRIER

##### A. Measurement configuration

The initial investigation of a noise barrier with profile scanning was limited to a single post (steel beam with a double T profile) which has a height of approximately 5 m. The measurement configuration is depicted in Figure 1 and as a schematic cross section in Figure 7.

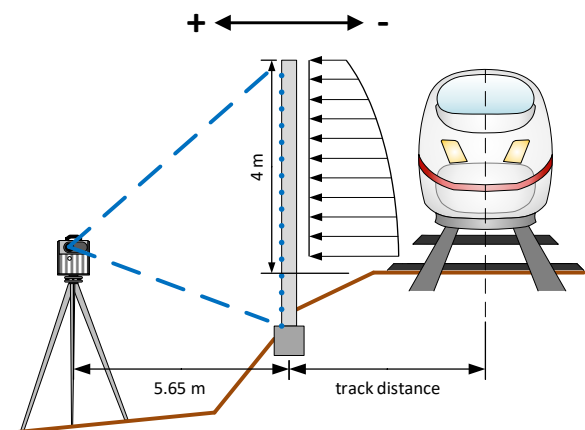


Figure 7. Measurement configuration and schematic load situation across the train track.

The horizontal distance between consecutive posts at the monitoring location is 5 m and the height of the noise barrier above the rail level is approximately 4 m. Each area between consecutive posts is closed with two noise protection elements (prefabricated concrete parts, each one approximately 2 m high). Underneath the prefabricated noise protection elements is a component of solid reinforced concrete, see Figure 1.

**B. Load situation due to the passing train.**

A moving train creates a pressure field that is firmly connected to the train and consists of sections of high and low pressure that follow each other at short intervals, see Figure 8. The main parts of this pressure field are at the head and tail of the train: the head induces a rapid change from pressure to suction, while the tail of the train causes a change from suction to pressure. Those dynamically changing load impulses can stimulate noise barriers to vibration.

Figure 8 shows a schematic representation of a high speed train with the indicated pressure field in blue and red. The diagram is supplemented with an exemplary analytical load diagram according to the guideline (DB RIL 804.5501, 2007). In addition Figure 7 shows the situation in the cross section indicating the decreasing pressure due to the height above track level at the noise barrier.

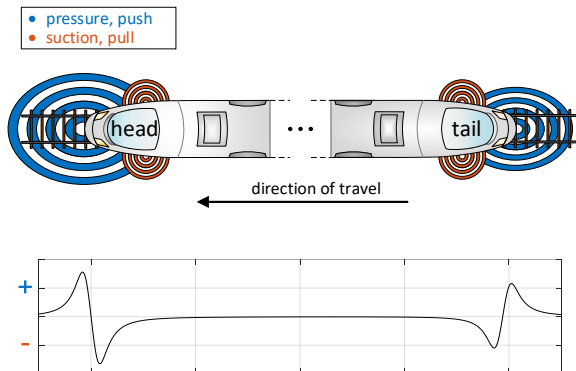


Figure 8. Pressure field and the related analytical load diagram along the train.

The overall pressure increases with the square of the train speed, but decreases again with the distance from the track axis and the height above the track level, see (Niemann and Hölscher, 2009).

The pressure/push or suction/pull on a point at the noise barrier therefore depends on the relative position of the train, the speed of the train, the track distance, the absolute height of the noise barrier, the vertical position at the noise barrier and the shape of the train.

All those parameters are taken into account for the calculation of the analytical load diagram according to the guideline (DB RIL 804.5501, 2007), which is valid for the Deutsche Bahn AG (DB) in Germany.

**C. Pre-processing of the profile scanner measurements with B-splines**

Since the surface geometry of the measured post is very smooth, in addition to the spatial clustering (see section 3), the measurement profiles can be approximated by free-form curves, especially the so-called base splines (B-splines), e. g. (Neuner et al., 2013; Bureik et al., 2016; Schill, 2018).

B-Splines consist of piece wise, polynomial functions of a defined degree. The creation of a B-spline requires control points, to which the B-spline converges due to the usage of weight functions (= basic functions) and so called nodes, where the polynomial functions are assembled.

The goal is to generate a curve that is as optimally adjusted as possible, passes close to the checkpoints and can be modified locally by changing the checkpoint positions. Since a spline curve is clearly defined by the two parameters nodes and checkpoints, the definition and manipulation of B-splines can always be traced back to the determination of suitable nodes and checkpoints, e. g. (Schmitt and Neuner, 2015; Harmening and Neuner, 2016).

Figure 9 shows an exemplary profile of the measured post with the B-spline approximation in the left diagram and for comparison the spatial clustering in the right diagram. For both methods the approximation was limited to the area from -0.4 m up to 3.8 m, since this area represents approximately the part of the noise barrier above the track level.

The discretisation of the B-spline allows the derivation of deformation time series at any given position in the approximated area. In the following section the time series of the discretised B-splines are used for the deformation monitoring of the noise barrier.

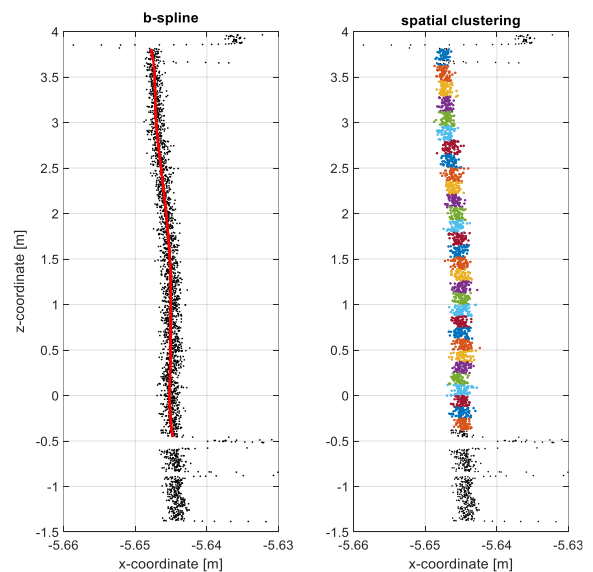


Figure 9. Example of the applied approximation methods.

#### D. Results of the initial investigation

In the following the time-dependent deformations of a post of a noise barrier due to the passing of two trains are presented: a TGV Euroduplex high-speed double decker train and an ICE-S, each with a speed of approximately 250 km/h.

The stability of the profile scanner during the measuring periods was monitored and confirmed with stable areas in the scanned profiles (possible due to the 360 degree scan range). For the monitoring of this noise barrier, the verification could be performed with a measurement uncertainty between 0.1 mm and 0.2 mm. In cases in which this is not possible, it is an option to use accelerometers and/or inclination sensors to verify the stability of the profile scanner.

To compare the analytical load assumptions with the time-dependent deformations, the load diagram from Figure 8 was transformed into time series according to the speed and length of the trains. The result represents the theoretical force acting on a single point at a defined height over the track level on the noise barrier in compliance with the guideline (DB RIL 804.5501, 2007), see upper diagrams in Figure 10 and Figure 11. The three curves illustrate the analytical load time series for exemplary heights above the track level: 0.7 m (blue), 2.2 m (red) and 3.7 m (yellow).

The three lower diagrams in Figure 10 and Figure 11 depict the corresponding deformations determined from profile scanner measurements at the same heights in the same colours for the two different trains. The sign of the x-coordinate was chosen according to the theoretical introduced load, meaning that the positive sign is pointing away from the train track as depicted in Figure 7.

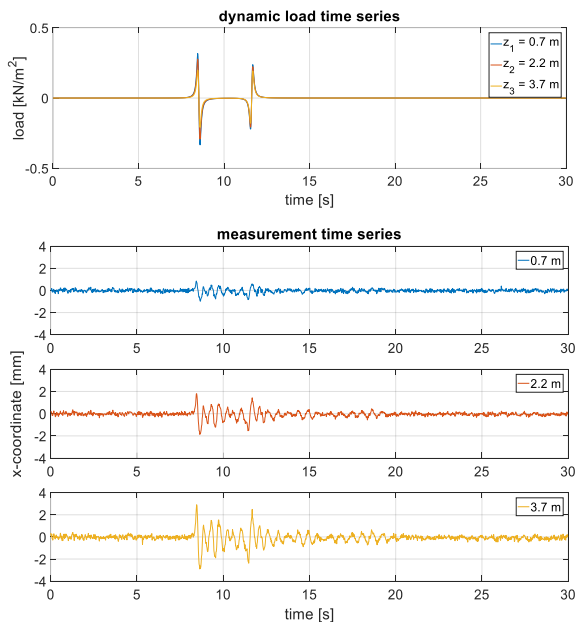


Figure 10. Time dependent analytical load diagram and the measured deformation output for a TGV.

All three exemplary deformation time series in Figure 10 show clearly the shape of the analytical load time series from the diagram above. The head and tail wave of the train induce the biggest deformations of up to 3 mm. Also the ratio between the deformation amplitudes due to the head and tail wave is fitting well to the analytical load assumptions. In addition the noise barrier is beginning to vibrate with a frequency of about 2 Hz because of the train passing.

The second train depicted in Figure 11 induces even bigger deformations of up to 4 mm, due to the pressure of the head wave. The ratio between the main deformation amplitudes does not fit as good as with the TGV passing. The most likely reason is that due to the different length of the train, vibrational effects superimpose with the deformation due to the tail wave, leading to larger absolute values of deformation.

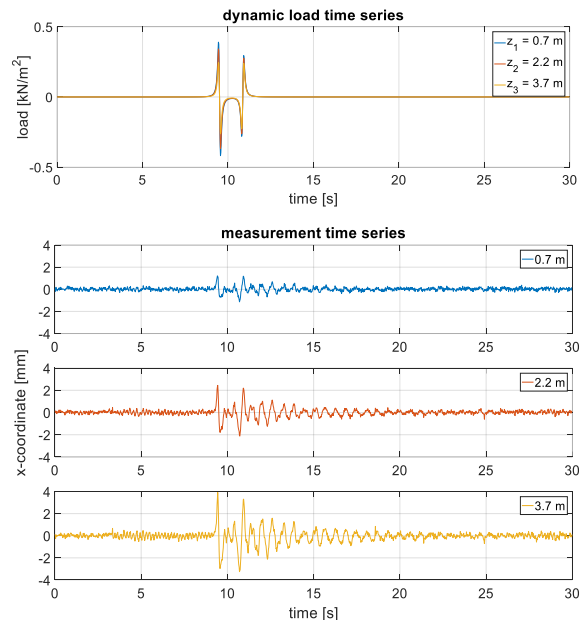


Figure 11. Time dependent analytical load diagram and the measured deformation output for an ICE-S.

In addition to the vibration of about 2 Hz, as seen also in the diagrams of Figure 10, there is another frequency content of 5.5 Hz beginning approximately 5 seconds before the head wave hits the post of the noise barrier. This effect is seen only in the lower two diagrams (heights 2.2 m and 3.7 m) of Figure 11 and corresponds to the scale of typical natural frequencies of noise barriers (Niemann and Hölischer, 2009; Grimm et al., 2012). To further evaluate its origin will be a goal for future investigations.

#### V. CONCLUSIONS

The presented deformation monitoring of a noise barrier with a profile scanner demonstrates that a non-contact measuring system can capture temporally variable structural deformations more efficiently and in a much higher spatial resolution than conventional sensors for the monitoring of supporting structures.

Furthermore it is possible to reach measurements uncertainties of nearly the same scale as generated with classical discrete measurement sensors, due to the presented measurement and evaluation methodology.

The spatio temporal processed data basis allows the derivation of deformations at nearly any desired position within a measurement profile (post mission). Therefore the dependence on prior knowledge about the structure or on the theoretical deformation behaviour is greatly reduced. That applies to the measurement planning as well as the analysis.

Future work will concentrate on the numerical modelling of the noise barrier structure and in this context to utilize the adaptable spatial resolution of the profile scanner to validate the resulting structure model.

#### REFERENCES

- Bureick, J., H. Alkhatib, and I. Neumann (2016). Robust Spatial Approximation of Laser Scanner Point Clouds by Means of Free-form Curve Approaches in Deformation Analysis. *Journal of Applied Geodesy*. Vol. 10, Issue 1, pp. 27–35, doi: 10.1515/jag-2015-0020
- Deutsche Bahn (2007). Richtlinie 804.5501: Bautechnik, Leit-, Signal- u. Telekommunikationstechnik, Eisenbahnbrücken u. sonstige Ingenieurbauwerke, Lärmschutzanlagen an Eisenbahnstrecken
- Firus, A., J. Schneider, H. Berthold, M. Albinger, A. Seyfarth (2018). Parameter identification of a biodynamic walking model for human-structure interaction. In: *Proc. of 9th Int. Conf. on Bridge Maintenance, Safety and Management*. Power N Frangopol D M Al-Mahaidi R Caprani C (eds). 09.–13.07.2018 in Melbourne (Australia), pp. 668–674, doi: 10.1201/9781315189390
- Grimm, R., P. Limper, and C. Seiler (2012). Quasi-statische und dynamische Berechnungen zum Tragverhalten von Lärmschutzwänden der Deutschen Bahn AG. *Bauingenieur*. Vol. 87, Issue 5, pp. 237–243, issn: 0005-6650
- Harmening, C. and H. Neuner (2016). Choosing the Optimal Number of B-spline Control Points (Part 1: Methodology and Approximation of Curves). *Journal of Applied Geodesy*. Vol. 10, Issue 3, pp. 139-157, doi: 10.1515/jag-2016-0003
- Hoffmeister, B. (2007). Lärmschutzwände an Hochgeschwindigkeitsstrecken der Bahn – eine Herausforderung für den Leichtbau. In: *Proc. of D-A-CH Tagung der Österreichischen Gesellschaft für Erdbebeningenieurwesen und Baudynamik*. 27.–28.09.2007 in Vienna (Austria)
- Hwang, J., H. Yun, S.-K. Park, D. Lee, S. Hong (2012). Optimal Methods of RTK-GPS/Accelerometer Integration to Monitor the Displacement of Structures. *Sensors*. Vol. 12, Issue 1, pp. 1014–1034, doi: 10.3390/s120101014
- Neitzel, F., T. Schwanebeck, and W. Schwarz (2007). Zur Genauigkeit von Schwingwegmessungen mit Hilfe von Beschleunigungs- und Geschwindigkeitssensoren. *AVN Allgemeine Vermessungs-Nachrichten*. Vol. 114, Issue 6, pp. 202–211, issn: 0002-5968
- Neuner, H., C. Schmitt, and I. Neumann (2013). Modelling of terrestrial laser-scanning profile measurements with B-Splines. In: *Proc. of 2nd Joint international Symposium on Deformation Monitoring (JISDM)*. 09.–12.09.2013 in Nottingham (UK)
- Niemann, H.-J., and N. Hölscher (2009). Eigendynamik unerwünscht. In: *Wissenschaftsmagazin Rubin der Ruhr-Universität Bochum, Sonderheft des Wissenschaftsmagazins RUBIN zum Sonderforschungsbereich 398 „Lebensdauerorientierte Entwurfskonzepte unter Schädigungs- und Deteriorationsaspekten“*. pp. 34–41, issn: 0942-6639
- Schill, F., and A. Eichhorn (2016). Investigations of low- and high-frequency movements of wind power plants using a profile laser scanner. In: *Proc. of 3rd Joint International Symposium on Deformation Monitoring (JISDM)*. 30.03.–01.04.2016 in Vienna (Austria)
- Schill, F. and A. Eichhorn (2017). Automatische Segmentierung von Profilschannermessungen am Beispiel von Brückenbauwerken. In: *Ingenieurvermessung 17 – Beiträge zum 18. Int. Ingenieurvermessungskurs*. Lienhart W (eds). 25.–29.04.2017 in Graz (Austria), pp. 389–401, isbn: 978-3-87907-630-7
- Schill, F. (2018). Überwachung von Tragwerken mit Profilschannern. Deutsche Geodätische Kommission (DGK), Reihe C, Nr. 820, isbn: 978-3-7696-5231-4, identical with TUpriints-E-Publishing-Service der TU Darmstadt urn:nbn:de:tuda-tupriints-72679, uri: http://tupriints.ulb.tu-darmstadt.de/7267
- Schmitt, C. and H. Neuner (2015). Knot estimation on B-Spline curves. *Österreichische Zeitschrift für Vermessung & Geoinformation*. Vol. 103, Issue 2 + 3, pp. 188–197, issn: 1605-1653
- Schulte-Werning, B., M. Beier, K.G. Degen, D. Stiebel (2006). Research on noise and vibration reduction at DB to improve the environmental friendliness of railway traffic. *Journal of Sound and Vibration*. Vol. 293, Issues 3–5, pp. 1058–1069, doi: 10.1016/j.jsv.2005.08.065
- Thompson, D. (2008). Railway noise and vibration: mechanisms, modelling and means of control. *Elsevier Science*, isbn: 978-0-0804-5147-3
- Tokunaga, M., M. Sogabe, T. Watanabe, T. Santo, S. Tamai (2014). Dynamic response characteristics of the tall noise barrier on railway structures during passage of trains and its design method. In: *Proc. of the 9th International Conference on Structural Dynamics, EURO-DYN 2014*. Cunha A Caetano E Ribeiro P. Müller G. (eds). 30.06.–02.07.2014 in Porto (Portugal), pp. 3761–3768, issn: 2311-9020, isbn: 978-972-752-165-4
- u-blox (2019). LEA-6 u-blox 6 GPS Modules Data Sheet. [https://www.u-blox.com/sites/default/files/products/documents/LEA-6\\_DataSheet\\_\(UBX-14044797\).pdf](https://www.u-blox.com/sites/default/files/products/documents/LEA-6_DataSheet_(UBX-14044797).pdf) [18.02.2019]
- Wujanz, D., J.-A. Paffenholz, F. Schill, M. Burger, U. Stenz, R. Lichtenberger, F. Neitzel, A. Eichhorn, I. Neumann (2018). Terrestrisches Laserscanning für die Überwachung von Brücken bei Belastungsversuchen. In: *Mauerwerkskalender 2018 Brücken, Bauen im Bestand*. Jäger W (eds). Ernst & Sohn: Berlin, pp. 221-239, isbn: 978-3-433-03181-0
- Zoller + Fröhlich (2019). Z+F PROFILER® 9012 Data sheet. [https://www.zf-laser.com/fileadmin/editor/Datenblaetter/Z\\_F\\_PROFILER\\_9012\\_Datasheet\\_E\\_final\\_compr.pdf](https://www.zf-laser.com/fileadmin/editor/Datenblaetter/Z_F_PROFILER_9012_Datasheet_E_final_compr.pdf) [18.02.2019]